# Spray Layer-by-Layer Electrospun Composite Proton Exchange Membranes

*David S. Liu, J. Nathan Ashcraft, Matthew M. Mannarino, Meredith N. Silberstein, Avni A. Argun, Gregory C. Rutledge, Mary C. Boyce, and Paula T. Hammond**

**Polymer electrolyte films are deposited onto highly porous electrospun mats using layer-by-layer (LbL) processing to fabricate composite proton conducting membranes. By simply changing the assembly conditions for generation of the LbL film on the nanofiber mat substrate, three different and unique composite film morphologies can be achieved in which the electrospun mats provide mechanical support; the LbL assembly produces highly conductive films that coat the mats in a controlled fashion, separately providing the ionic conductivity and fuel blocking characteristics of the composite membrane. Coating an electrospun mat with the LbL dipping process produces composite membranes with "webbed" morphologies that link the fibers in-plane and give the composite membrane in-plane proton conductivities similar to that of the pristine LbL system. In contrast, coating an electrospun mat using the spray-LbL process without vacuum produces a uniform film that bridges across all of the pores of the mat. These membranes have methanol permeability similar to free-standing poly(diallyl dimethyl ammonium chloride)/sulfonated poly(2,6-dimethyl 1,4-phenylene oxide) (PDAC/sPPO) thin films. Coating an electrospun mat with the vacuum-assisted spray-LbL process produces composite membranes with conformally coated fibers throughout the bulk of the mat with nanometer control of the coating thickness on each fiber. The mechanical properties of the LbL-coated mats display composite properties, exhibiting the strength of the glassy PDAC/sPPO films when dry and the properties of the underlying electrospun polyamide mat when hydrated. By combining the different spray-LbL fabrication techniques with electrospun fiber supports and tuning the parameters, mechanically stable membranes with high selectivity can be produced, potentially for use in fuel cell applications.**

## 1. Introduction

The development of thin solid polymer electrolytes with improved performance is critical for the advancement of electrochemical energy devices.[1] In recent years, considerable interest has been focused on designing chemically and mechanically stable membranes while maintaining high ionic conductivity with low fuel crossover.[2] For hydrogen and direct-methanol fuel cells, membranes comprising perfluorosulfonic acid polymers such as Nafion have been used because they exhibit superior protonic conductivity with relatively high mechanical integrity and chemical stability, despite their high cost.[3] However, even the perfluorosulfonic acid polymers have shown limited device lifetimes due to chemical and mechanical degradation.[4–8] One of the main causes of membrane failure is the poor dimensional stability, caused by repeated swelling/deswelling of the membrane in a fuel cell from the cycling of temperature and humidity, which has been shown to mechanically weaken the membrane after only a few hundred cycles.[9–12] Typically, to improve the membrane's mechanical properties, the ionomer (Nafion) is incorporated into dimensionally stable supporting matrices such as expanded polytetrafluoroethylene (ePTFE).[4,13–16] Other researchers have tried incorporating carbon nanotubes, metal oxides, and zirconium phosphates into Nafion matrices to improve lifetime or cell performance.[17–19]

The difficulty with these bulk composites is the lack of control of composition on the micrometer-scale and the continued reliance on Nafion, with its high cost and relatively high fuel crossover, in particular for methanol. A promising approach is to combine two relatively new processing techniques, layer-by-layer (LbL) assembly of polymer thin films and electrospinning of fiber mats. LbL assembly is an extremely versatile nano-scale fabrication technique that allows for the conformal coating of any wettable substrate with a combination of two or more polymers possessing complementary interactions, e.g., oppositely charged functional groups.[20–22] The films are generated

D. S. Liu, Dr. J. N. Ashcraft, M. M. Mannarino, Dr. A. A. Argun, Prof. G. C. Rutledge, Prof. P. T. Hammond
Department of Chemical Engineering
Massachusetts Institute of Technology
Room 76-553, 77 Massachusetts Ave,
Cambridge MA 02139, USA
E-mail: Hammond@mit.edu
Dr. M. N. Silberstein, Prof. M. C. Boyce
Department of Mechanical Engineering
Massachusetts Institute of Technology
Cambridge, MA 02139, USA

**DOI: 10.1002/adfm.201202892**

through the alternating adsorption of polyanions and polycations, and can be further tuned by adjusting the pH or adding salt to the polymer solutions during assembly, with typical thickness per bilayer ranging from a few nanometers to over a hundred nanometers. Farhat et al. and Argun et al. recently reported LbL-based proton exchange membranes (PEMs) with high performance in hydrogen and direct methanol fuel cells.[23,24] Further work by Ashcraft et al. showed that the LbL system composed of poly(diallyl dimethyl ammonium chloride) (PDAC) and sulfonated poly(2,6-dimethyl 1,4-phenylene oxide) (sPPO), structures shown in **Figure 1**a, yielded the highest protonic conductivity of any LbL assembled system, as high as 70 mS $cm^{-1}$, which is on the order of Nafion's conductivity, with methanol permeability values less than one hundredth that of Nafion;[25] however, these LbL-based PEMs are not sufficiently strong when hydrated and require a reinforcing mechanical substrate.

An interesting class of materials for reinforcing LbL membranes is the electrospun fiber mat. Electrospun mats are non-woven, highly porous materials with high surface-to-volume ratios and small pore sizes relative to other fibrous materials.[26–29] A wide range of polymers can be formed into electrospun mats, and the fiber diameters can be varied during fabrication over a wide range (0.1–10 μm).[29] Electrospinning has been used to produce high proton conductivity fibers from perfluorosulfonic acid (PFSA) and polyethylene oxide (PEO) into mechanically robust membranes;[30] however, a non-swelling, mechanically stable nanofiber mat could also serve as a porous scaffold for deposition of a conducting medium. Figure 1b shows a diagram illustrating the steps by which a composite membrane can be fabricated by either dip-LbL or spray-LbL application of polyelectrolytes to an electrospun nanofiber mat. The spray-assisted LbL process enables the coating of complex and porous surfaces, while also significantly reducing the cycle times for multilayer assembly from several minutes to a few seconds, thus making the LbL approach commercially viable.[31] In a recent publication we demonstrated that the spray-LbL process can be used to generate LbL-coated electrospun mats.[32] The fibers were shown to be individually coated throughout the interior of the mat when assembled with the assistance of a vacuum to control flow through the mat. In the absence of a vacuum, a condensed thin film was found to form at the surface of the mat, resulting in asymmetric composite membranes. This work demonstrated the versatility of combining the spray-LbL assembly process with electrospun mats.

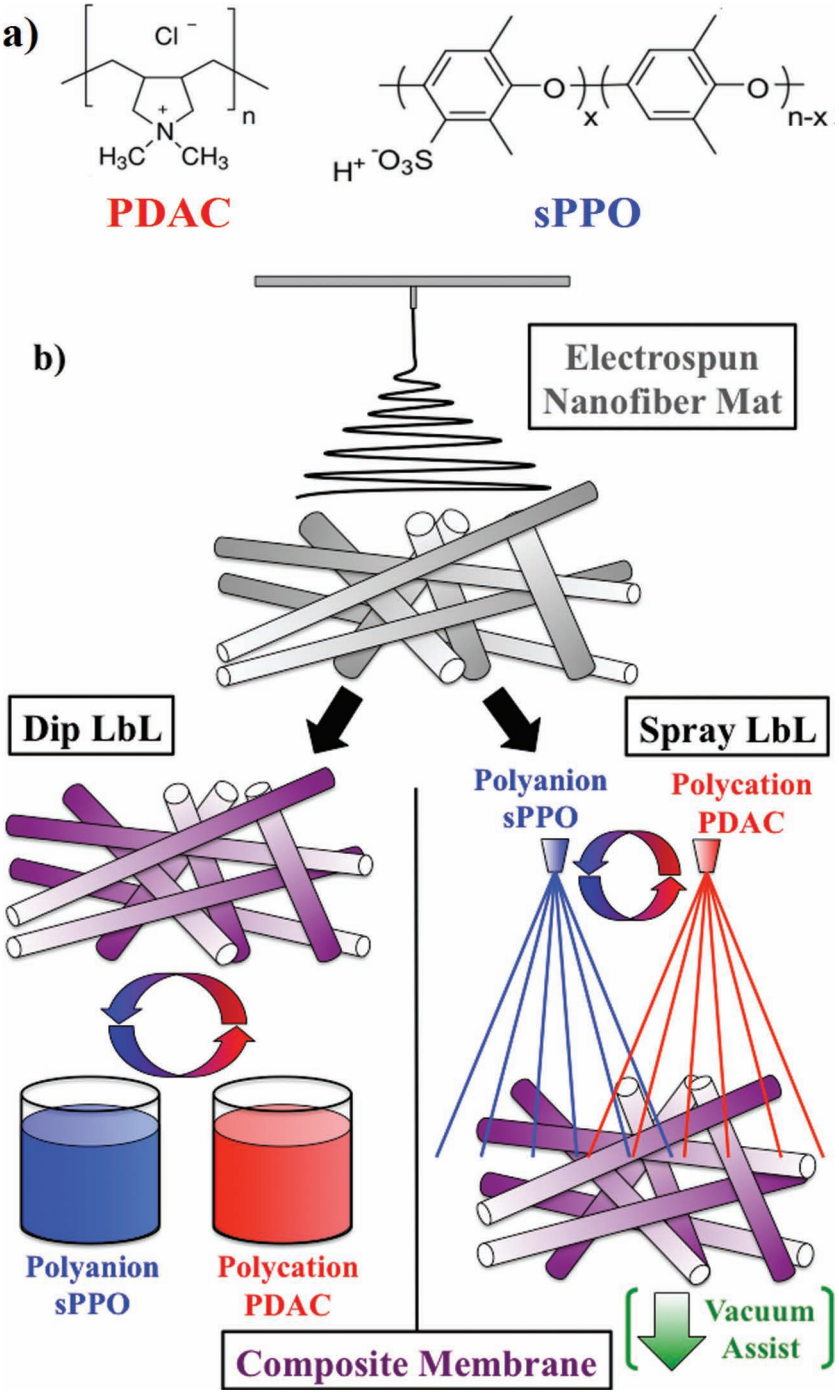


**Figure 1.** a) Chemical structures of PDAC and sPPO. These two polymers are combined in the LbL assembly process to yield highly conductive PEMs. b) Schematic diagram showing the fabrication process of LbL-fiber composite membranes by both dip and spray processes.

Here we demonstrate the mechanical enhancement of LbL membrane systems with the use of electrospun mats as substrate materials. Specifically, LbL assembly is used to generate selective coatings on and within the electrospun mats, producing thin, mechanically stable composite fuel cell membranes

for high power density devices. These material systems can be modified at the molecular level to alter transport properties, simply by changing the relative compositions of each adsorbed bilayer of polymer, while the mechanical and chemical stability can be modified by altering the nature or composition of the underlying electrospun network; the systems are highly controllable and the architectures of the films are modified across the thickness to achieve mechanically robust, highly selective, and readily processable ultrathin fuel cell membranes, with the goal of rivaling or exceeding the performance of Nafion. To demonstrate this, we explore in this report three different LbL assembly techniques: traditional dip-LbL, which involves directly dipping into alternate polyelectrolyte solutions, spray-LbL, and vacuum-assisted spray-LbL. We observe that each of these three techniques create distinctively different nanometer to micron scale morphologies on the fiber scaffold, each contributing different membrane characteristics. The mechanical properties of the composites are investigated, as well as other key properties for a methanol PEM: protonic conductivity and methanol permeability. Poly(trimethyl hexamethylene terephthalamide) (PA 6(3)T) and polycaprolactone (PCL) electrospun mats are used for their range of fiber sizes (200 nm to 10 μm). The dip-LbL electrospun composite membranes are shown to yield morphologies with less controlled bridging and linking of fibers together. The spray-LbL electrospun composite membranes consist of surface top-coatings that do not penetrate into the bulk of the mat. On the other hand, when a vacuum is pulled across the electrospun mat during spray-LbL assembly, the process yields conformal coatings of the individual fibers with minimal bridging throughout the bulk of the mat. The mechanical properties of the spray-LbL electrospun mats are shown to be superior to the pristine LbL free-standing films previously studied.

## 2. Results and Discussion

### 2.1. Mechanical Properties of Dipped Layer-by-Layer Films

Stress-strain curves of free-standing PDAC/sPPO films are shown in **Figure 2** for both ambient (dry) and fully hydrated (wet) conditions. It has previously been shown that dry PDAC/sPPO films have higher elastic moduli and strain-to-break than dry pristine sPPO, an indication that the LbL polyelectrolyte complex films are more mechanically durable than sPPO alone.[25] The dry, free-standing PDAC/sPPO films exhibit elastic-plastic behavior with elastic modulus values ranging from 250–1100 MPa and yield stress values ranging from 4–40 MPa depending on the processing conditions. LbL assembly at higher salt concentrations forms a more compliant network due to ionic shielding and a lower effective ionic crosslink density, resulting in films with lower elastic modulus and higher yield stress values than films assembled with lower or no salt concentrations, which form highly cross-linked, rigid materials. Overall, under dry conditions, the elastic modulus and yield stress values of PDAC/sPPO compare well with those of Nafion, which has an elastic modulus of 300 MPa and a yield stress of 12 MPa.[33] However, the

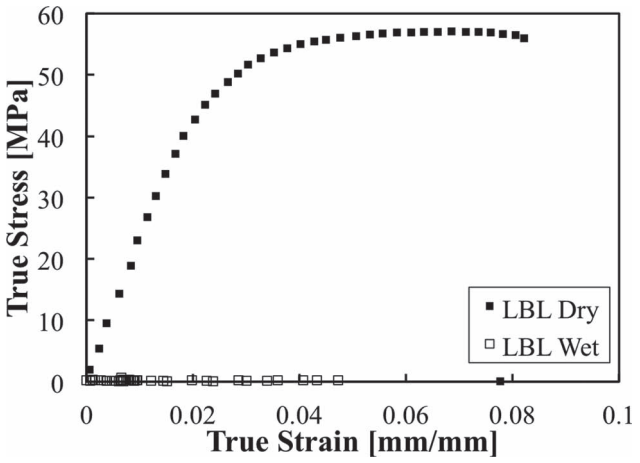


**Figure 2.** Typical stress-strain curves for free-standing PDAC/sPPO films at ambient (dry) and fully humidified (wet) conditions. The PDAC/sPPO films were assembled at pH = 1.0 with 0.5 M NaCl in the sPPO assembly solution. The films were sprayed onto a polystyrene coated silicon wafer and gently removed after assembly.

layer-by-layer films become brittle when dry and tear at small strains. The average true strain-to-break of free-standing PDAC/sPPO films is 0.07, which compares unfavorably to a true strain-to-break greater than 1.0 for Nafion under dry conditions. Under hydrated conditions the PDAC/sPPO free-standing films become almost gel-like, and the mechanical strength is lower than the detection threshold of the extensometer. At the hydrated operating conditions of a fuel cell, these mechanical values would lead to very short MEA lifetimes due to mechanical failure of the membrane. These results motivated the development of electrospun mats as reinforcing substrates in this work.

### 2.2. Dipped Layer-by-Layer Electrospun Composite Films

**Figure 3** shows SEM images of PCL electrospun mats coated through the dip-LbL assembly process; electrospun mats with 0, 50, 125, and 250 bilayers (BLs) of PDAC/sPPO film are shown. The uncoated PCL electrospun mats have mean fiber diameter of 8.6 μm as shown in Figure 3a. Figure 3b–d show that the fibers become coated as more bilayers of PDAC/sPPO are applied to the PCL mats, but the multilayers form webbed thin films that bridge across the various fibers even at low numbers of bilayers. This webbed morphology is unique to dip-LbL assembly. It is believed to be the result of full water immersion followed by long vertical drain times associated with dipping, which permits the formation of a polymer film joining two fibers starting at their intersection but not bridging across all the fibers in one uniform film. Meanwhile, the fibers that aren't webbed continue to be coated with PDAC/sPPO film and grow thicker until webbing eventually occurs. The result is a surface coating that has a propensity to bridge at fiber intersections and yields a non-uniform, partially-bridged morphology. LbL films of PDAC/sPPO fabricated at the same assembly conditions on a planar glass substrate grow at a rate of 24.0 nm/BL;

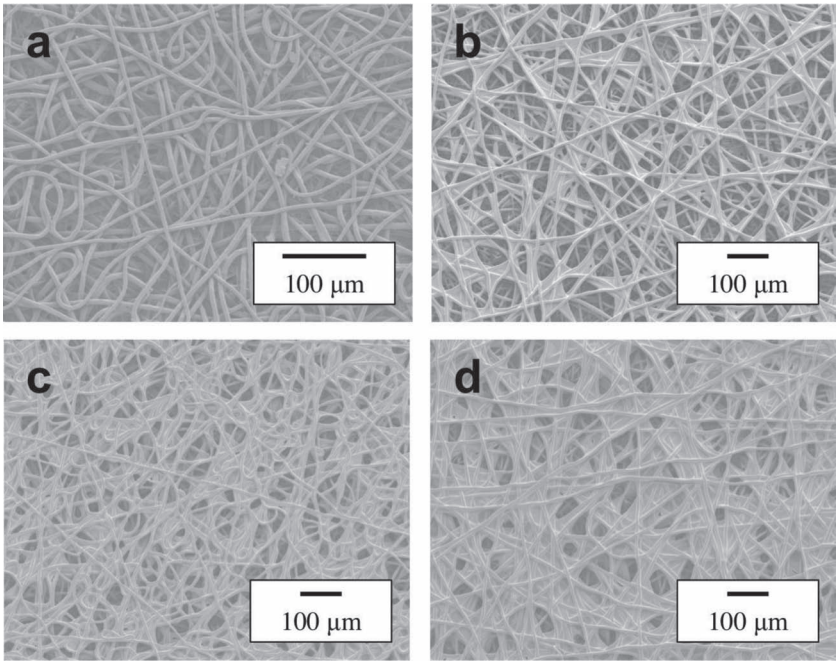


**Figure 3.** SEM images of PCL electrospun mats coated using dip-LbL with a) 0 BLs, b) 50 BLs, c) 125 BLs, and d) 250 BLs of PDAC/sPPO. PCL electrospun mats have mean fiber diameter of 8.6 μm. PDAC/sPPO deposition conditions are pH = 1.0, 0.5 M NaCl in sPPO, and no salt in PDAC or any rinse solutions. Scale bar for each SEM micrograph is 100 μm.

therefore, a 50-BL deposition of PDAC/sPPO corresponds nominally to a 1.2 μm film thickness, and a 250-BL deposition of PDAC/sPPO corresponds nominally to 6 μm in thickness. From Figure 3b (50 BLs) and Figure 3d (250 BLs), the fibers, particularly those on the top layers, appear to grow in diameter by about 2.4 μm and 12 μm, respectively, while the bridging films connect more fibers with additional layers. A continuous coating that prevents fuel crossover could be achieved with a sufficient number of bilayers; however, the processing time for such a composite membrane would be on the order of weeks with this dip-LbL method. In addition it was observed by cross-sectional SEM that the multilayer film did not fully penetrate into the interior of the electrospun mat. This results in a gradient in coating across the thickness of the membrane, which is expected to lead to anisotropy in the ionic conductivity of the composite membrane.

The in-plane protonic conductivity values of PCL electrospun mats coated with 125 and 250 BLs of PDAC/sPPO are shown in **Figure 4**, along with a PDAC/sPPO film assembled on a glass slide. As the number of bilayers deposited on the electrospun mat increases, the number of webbed bridges increases and the total in-plane protonic conductivity of the composite membrane increases. It appears that by 250 BLs, all of the coated fibers have been connected and the protonic conductivity of the composite approaches that of PDAC/sPPO; however, due to the lack of penetration into the electrospun mat, the void space in the center of the mat is not completely filled. The slope of the composite membrane conductivity with humidity, particularly of the 125-BL dipped electrospun mat, is the same as that of the PDAC/sPPO-only film, indicating the same mechanism of ion transport through the composite.

### 2.3. Spray-LbL Electrospun Composite Films

To further investigate the potential to achieve highly conductive composite membranes, an improved methodology was adopted. PCL is biodegradable and hydrolytically unstable, so the more durable, hydrolytically stable PA 6(3)T was selected for producing electrospun mats for the remaining studies. PA 6(3)T fiber diameters can be varied from 2 μm down to 0.2 μm. With spray-LbL, it is possible to achieve both pore filling and covering of pores at the surface by using two different spray conditions. Pore filling is achieved when a vacuum is drawn on the downstream side of the electrospun mat during the vacuum-assisted spray-LbL process, effectively coating each fiber through the entirety of the mat. By contrast, a superficial film on both sides of the mat is achieved by simply turning off the vacuum during the spraying process and flipping over the mat to cover both sides of the membrane. **Figure 5** shows the electrospun mats used prior to any spray coating process; the mean fiber diameter is 1.24 μm.

To fill the electrospun mat uniformly and improve through-plane conductivity, a vacuum was applied to the downstream side of the mat during assembly, allowing a highly conductive matrix to be electrostatically connected to the supporting mat. Representative SEM images of the spray-coated electrospun PA 6(3)T mats with and without vacuum are shown in **Figure 6**. Figure 6a,b show images at two different magnifications of an electrospun mat coated with 250 bilayers of PDAC/sPPO with a vacuum applied

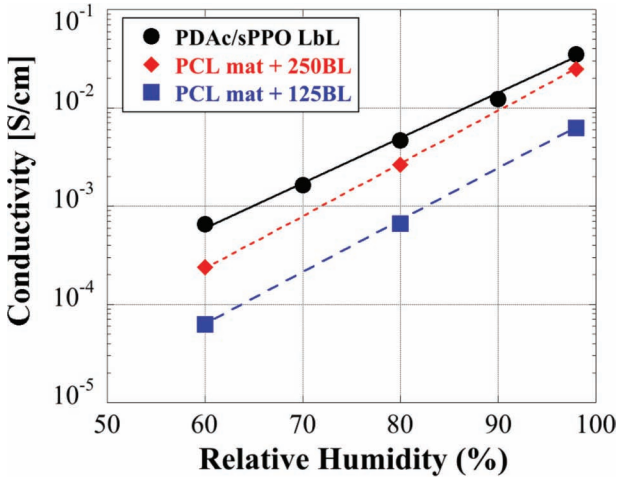


**Figure 4.** Relative humidity dependence of in-plane protonic conductivity of PDAC/sPPO films coated on PCL electrospun mats. PDAC/sPPO deposition conditions are pH = 1.0, 0.5 M NaCl in sPPO, and no salt in PDAC or any rinse solutions. As the number of bilayers deposited on the electrospun mat increases, the webbing of the PDAC/sPPO helps link all of the coated fibers and a large increase in conductivity is observed.

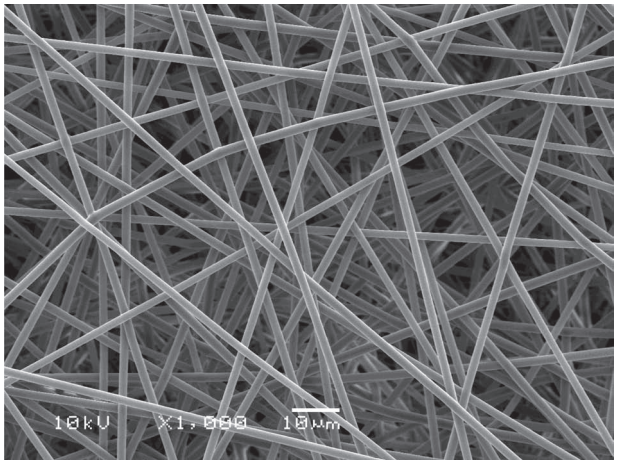


**Figure 5.** SEM micrograph of a PA 6(3)T electrospun mat having mean fiber diameter of 1.24 µm. The scale bar for the micrograph is 10 µm.

to the back of the mat. When sprayed under vacuum, the individual fibers of the mat are coated conformally, as the deposition occurs below the critical Reynolds number for flow separation from the downstream side of a cylinder[34] using conditions similar to those previously reported.[30] As can be seen in Figure 6a, the vacuum-assisted spray-LbL process produces fibers that are smoothly, uniformly, and individually coated with minimal pore blockage. The polyelectrolyte solution is pulled across the entire thickness of the electrospun mat and thus all the fibers, not just those near the surface, are coated. The charged surface of the PA 6(3)T fibers caused by plasma-treatment increases the wettability of the mat and provides an anionic substrate for LbL adhesion. The result is that the LbL penetrates through the void spaces and conformally deposits smooth and uniform LbL films around each fiber. From Figure 6b, it is observed that the growth of the multilayer film on the fibers (5.6 ± 0.4 nm/BL) is almost identical to the growth of the film on glass (6.1 nm/BL) under the same salt conditions, indicating a similar growth mechanism. The vacuum-assisted spray-LbL process enables uniform coating by eliminating webbing that would hinder the flow of the polymer solution droplets through the electrospun mat. The vacuum-assisted spray-LbL process allows the precise control of LbL film thickness on each fiber as well as the functional surface area and the degree of porosity of the composite film.

To create a film that covers all the pores in the supporting electrospun mat and drastically reduce the methanol permeability of the composite membrane, spray-LbL assembly without vacuum was applied to plasma-treated electrospun mats. When there is no vacuum applied during the spray deposition, the polymer solution droplets do not penetrate through the membrane, but instead form a pore-bridging film that spans across all the fibers along the top surface of the membrane. Figures 6c,d show images of an electrospun mat after spraying 100 BLs (2 µm) and 300 BLs (6 µm) with no vacuum, respectively. As can be seen in Figure 6c, with 100 BLs, the pores are covered, although the underlying PA 6(3)T fiber structure can still be seen. At 300 BLs, see Figure 6d, the LbL coating is so thick that the fibers (1.24 µm mean diameter) underneath are not visible anymore.

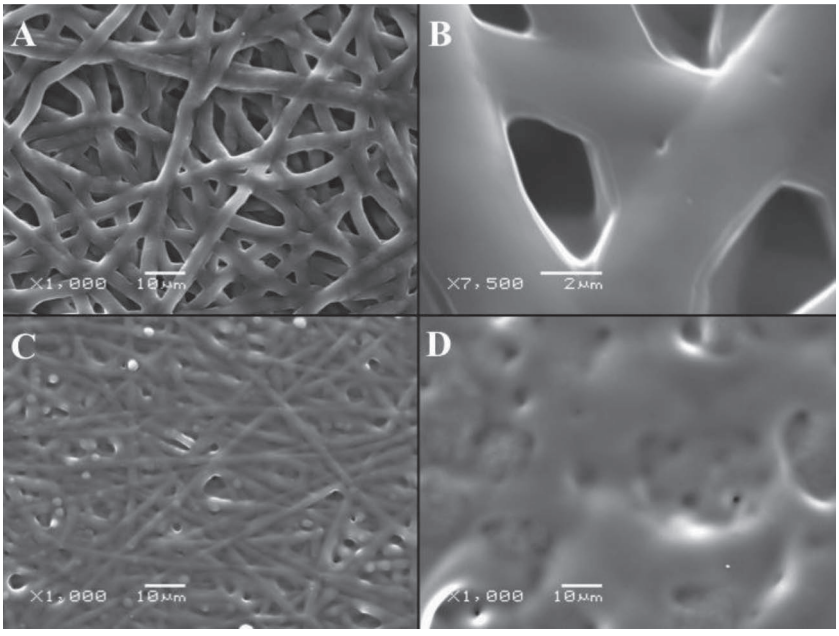


**Figure 6.** SEM images of a PA 6(3)T electrospun mat: a) front-side, b) zoomed in spray-LbL coated with 250 BLs of PDAC/sPPO, at pH2 with 0.5 M NaCl in the sPPO solution, when a vacuum is applied. The spray coatings provide a uniform coating on the fibers individually without webbing or pore covering. When there is no vacuum applied during the spray deposition, a pore-bridging film is observed after just 100 BLs (2.0 µm equivalent on glass) are sprayed at pH 2 with 1.0 M NaCl in all solutions (c). After 300 BLs (6.0 µm equivalent on glass) are deposited, the films have formed such a thick covering that it obscures the fibers underneath (d).

To probe the interior of the spray-coated electrospun mats, cross-sectional SEM images were obtained by cryofracturing the composite membranes in liquid nitrogen. **Figure 7**a shows the cross-section of a PA 6(3)T electrospun mat spray-coated with 175 BLs of PDAC/sPPO without vacuum. There is no penetration of the polymer solution into the electrospun mat, while the fibers underneath appear to be unaffected in any way. Figure 7b shows an electrospun mat spray-coated with 150 BLs of PDAC/sPPO with vacuum. For composite membranes prepared without vacuum, the LbL film starts growing at the surface, bridging across all the pores, and grows outward. For samples prepared with vacuum, Figure 7b shows that the individual fibers of the electrospun mat are coated throughout the film. The enlarged inset shows the conformal nature of the coating and how the LbL film on two adjacent fibers can merge. Because the LbL film grows on each fiber throughout the mat, just 150 BLs (0.5 µm) were enough to fill the majority of the void spaces of an 80-µm-thick membrane, reducing membrane porosity from 80% to 30% as measured gravimetrically based on the apparent density of

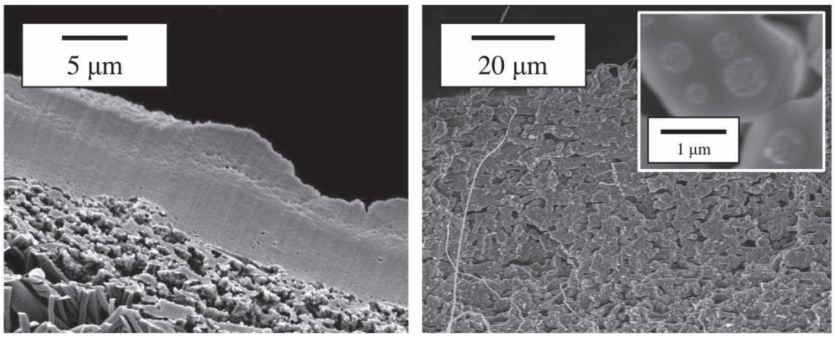


**Figure 7.** Cross-sectional SEM images of PA 6(3)T electrospun mats (mean fiber diameter of 0.46 ± 0.06 μm) spray coated with 175 BLs (6 μm) of PDAC/sPPO without vacuum (left) and spray coated with 150 BLs (0.5 μm) of PDAC/sPPO with vacuum (right and inset). Without vacuum, a pore-spanning film over the surface of the mat is formed, leaving the interior of the mat uncoated. With the application of a vacuum across the electrospun mat, the fibers of the mat are conformally coated throughout the mat. Scale bar for the left micrograph is 5 μm, scale bar for the right micrograph is 20 μm, and the scale bar for the inset is 1 μm.

the membrane and bulk density of the polymer. With further optimization, LbL electrospun composite membranes could be produced with even lower void space. However, an electrospun mat coated only with the vacuum-assisted spray-LbL process can never be completely filled with polyelectrolyte, and will be highly methanol permeable due to the remaining void space needed for the flow of air to be accommodated through the fiber mat. An improved composite membrane that conducts protons but rejects methanol can be formed by combining both types of spray-LbL techniques: the vacuum-assisted spray-LbL technique to fill the PA 6(3)T mat with conductive PDAC/sPPO, and the spray-LbL technique without vacuum to form a methanol barrier across the surface of the membrane.

### 2.4. Methanol Permeability Results

Methanol permeability was measured for spray-LbL electrospun mats to evaluate the effectiveness of the LbL films in reducing methanol crossover. When vacuum was applied during the spray-LbL process, the resultant composite membrane, with 30% void space, was highly permeable to methanol. However, when there was no vacuum applied during the spray-LbL process, the pore-bridging film was able to significantly reduce methanol permeability. **Figure 8** shows the methanol permeability of the composite membrane after a certain number of bilayers have been sprayed onto an electrospun mat without vacuum. With as little as 100 BLs (2 μm) on an 80-μm-thick electrospun mat, a fully bridged film is formed and the overall methanol permeability is already lower than that of Nafion. As seen in Figure 8, as the number of bilayers increases, a thicker LbL film is sprayed and the overall methanol permeability decreases. Thus, with the spray-LbL fabrication technique, the methanol permeability of the composite membrane may be varied.

To verify that the decrease in methanol permeability comes from the PDAC/sPPO pore-bridging top film on the electrospun mat and not from the bulk membrane, we compared the methanol permeability of the composite membranes with that of PDAC/sPPO supported on track-etched nucleopore membranes, as published previously.[24] **Table 1** lists the overall permeability of the composite membranes as well as the MeOH permeability of the LbL layer alone, assuming that it provides the sole barrier to MeOH crossover, measured for the composite membranes with different numbers of bilayers. The overall permeability is the measured rate of methanol crossover divided by the methanol concentration gradient (the change in concentration divided by the total thickness of the composite membrane comprising both LbL film and the electrospun mat). The permeability of the LbL layer alone is defined as the crossover divided by the methanol concentration gradient where only the thickness of the blocking LbL coating is used, ignoring the electrospun mat base. The thickness of the LbL coating on the fibers is estimated from the film growth curve as determined on a planar glass substrate and confirmed by cross sectional SEM. As seen in Table 1, the overall permeability of the composite membrane drops with increasing number of bilayers; however, the estimated permeability of the LbL layer remains the same, indicating that the inherent transport properties of the LbL film does not change with the number of bilayers. These numbers are similar to what was previously published on PDAC/sPPO films alone.[24] This proves that the primary blocking component for methanol crossover is a linearly growing PDAC/sPPO film on top of the electrospun mat.

### 2.5. Mechanical Behavior of the Composite Membranes

Monotonic and cyclic uniaxial tensile testing was performed on bare PA 6(3)T electrospun mats and vacuum-assisted, PDAC/sPPO spray-coated mats to assess the mechanical behavior of

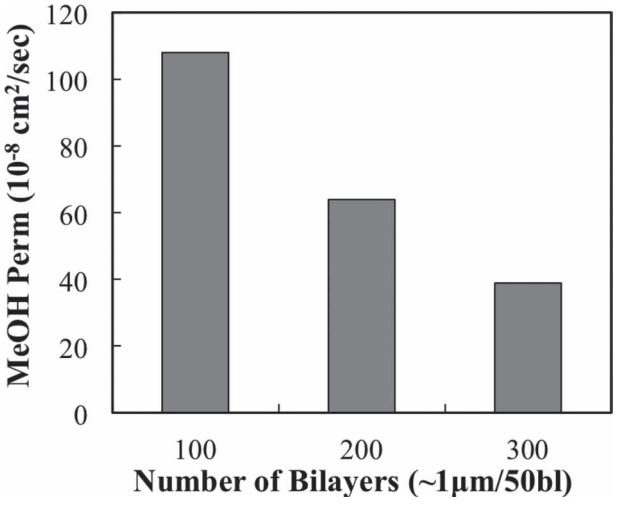


**Figure 8.** Methanol permeability of the composite membrane as a function of LbL film thickness for spray-coated electrospun mats. The spray conditions for the PDAC/sPPO films were pH = 2.0, 1.0 M NaCl in all solutions. As more bilayers are applied, the overall methanol permeability decreases.

**Table 1.** Methanol permeability of composite membranes with various numbers of bilayers of PDAC/sPPO.

| # of Bilayers | Overall Permeability [$10^{-8}$ $cm^2/s$][a)] | Thickness of LbL film [μm] | Estimated Permeability of LbL layer [$10^{-8}$ $cm^2/s$][b)] |
|---|---|---|---|
| 100[c)] | 108 | 2.0 | 2.7 |
| 200[c)] | 64 | 4.0 | 3.2 |
| 300[c)] | 39 | 6.0 | 2.9 |
| PDAC/sPPO film[24] | 2.18 | On Nucleopore | 2.18 |
| Nafion | 282 | N/A | N/A |

[a)]Defined as methanol flux multiplied by the total thickness of the membrane divided by the concentration difference across the membrane; [b)]Defined as methanol flux multiplied by thickness of blocking layer (LbL or Nafion) divided by the concentration difference across the membrane; [c)]Spray conditions: pH = 2, 1.0 M NaCl in all solutions without vacuum on a 75-μm thick electrospun mat.

these composite materials (**Figure 9**). Free-standing PDAC/sPPO films exhibit brittle elastic behavior with a Young's modulus up to 1100 MPa and a yield stress of 40–50 MPa under dry testing conditions. Uncoated PA 6(3)T electrospun mats exhibit elastic-plastic behavior with an elastic modulus ranging from 8–53 MPa and a yield stress ranging from 0.2–2 MPa. In cyclic testing the electrospun mats are seen to unload linearly at the same slope as the initial loading and to reload along nearly the same path, indicating little hysteresis. The electrospun mats are susceptible to necking and exhibit strains at break ranging from 0.3–1.0. The mechanical behavior of the PDAC/sPPO vacuum-assisted spray-coated electrospun mats is highly dependent upon the relative humidity, and maintains the characteristics of both the free-standing LbL and the bare mat. When the composite membrane is dry, the mechanical properties of the LbL film give the composite membrane a large elastic modulus with low strain-to-break. At failure, the LbL film component tears first, followed by yielding of the underlying electrospun mat. When the composite membrane is wet, the LbL provides minimal mechanical strength and the coated electrospun mat behaves like the bare PA 6(3)T mat as shown in Figure 9.

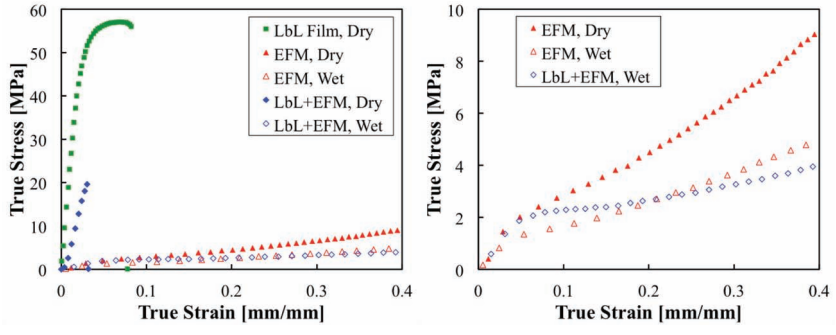


**Figure 9.** Stress-strain curves comparing free-standing LbL film to uncoated and vacuum-assisted spray-coated PA 6(3)T electrospun mats at ambient (dry) and fully humidified (wet) conditions. Shown to the full stress range of the LbL dry film (left). Shown at a lower stress range to better differentiate among the more compliant materials (right). The spray-coated mats exhibit composite membrane behavior; the LbL strengthens the mat when dry while the mat provides the supporting base when wet.

In observing the failure mechanisms of the coated mats after mechanical testing for both the dry and hydrated cases, it is seen that in the dry case, cracking occurs along the LbL surface, exposing the underlying electrospun mat, whereas in the hydrated case the surface layer is able to deform with the rest of the mat without cracking due to the ductile behavior of the LbL coating under hydrated conditions, as seen in bare film testing. Consequently, the spray coated mats exhibit superior mechanical properties as compared to the bare films, and are comparable to commercial proton exchange membranes. The mechanical properties of the underlying mat may be improved apart from LbL fabrication, thereby improving the structural properties of the composite membrane without affecting the key electrochemical properties of the LbL film, specifically methanol permeability and proton conductivity.

## 3. Conclusion

Composite membranes of highly conductive layer-by-layer (LbL) films and electrospun fiber mats are fabricated and characterized for mechanical strength and selectivity. The mechanical response of highly conducting PDAC/sPPO LbL films are improved by forming the LbL matrix on a highly controllable electrospun fiber scaffold. Free-standing PDAC/sPPO films have elastic moduli up to 1100 MPa and a maximum yield stress of 40 MPa. PDAC/sPPO films assembled with more salt in the assembly baths have better mechanical properties due to the more favorable cross-linked network that is formed. The mechanical properties of PDAC/sPPO are on par with commercial proton exchange membranes like Nafion at moderate to low relative humidity conditions; however, the PDAC/sPPO films break at extremely low strains (≈0.07 mm/mm) and become gel-like with low elastic modulus values when wet. Coating a PCL electrospun mat with the LbL dipping process produces composite membranes with interesting webbed morphologies that span adjacent fibers. The in-plane protonic conductivity of the composite membrane is similar to the pristine LbL system beyond a critical number of bilayers.

To create a fuel-blocking layer and to fill in more of the void space throughout the electrospun mat, the spray-LbL assembly is utilized as a means for the rapid formation of LbL films. When the spray-LbL technique is used along with an applied pressure gradient across the electrospun mat during assembly, the resulting LbL electrospun mat composites have conformal coatings on the individual fibers throughout the bulk of the mat. When the spray-LbL technique is used without vacuum, the resulting LbL film bridges across the pores of the electrospun mat, forming a continuous fuel-blocking layer with properties similar to the free-standing LbL film by itself. The mechanical properties of the spray coated electrospun mats are shown to be superior to the LbL-only system, particularly at hydrated conditions. This shows the versatility of the spray-LbL system to fabricate composite membranes

with finely tuned morphology and properties. Future studies are underway to model the mechanical behavior of the LbL electrospun composite membranes, and to develop future systems with increased mechanical durability as well as test the composite membrane in an operational direct methanol fuel cell.

## 4. Experimental Section

*Chemicals*: Poly(2,6-dimethyl 1,4-phenylene oxide) (PPO) (Mw = 23 000 g $mol^{-1}$) and polycaprolactone (PCL) (Mw = 80 000 g $mol^{-1}$) were obtained from Sigma-Aldrich, Inc. poly(diallyl dimethyl ammonium chloride) (PDAC) (Mw = 240 000 g $mol^{-1}$) was obtained from Polysciences, Inc. The amorphous polyamide poly(trimethyl hexamethylene terephthalamide), denoted PA 6(3)T, was obtained from Scientific Polymer Products, Inc. It has a glass transition temperature of 153 °C. N,N-dimethylformamide (DMF) was purchased from Sigma–Aldrich and used as received for creating polymeric solutions. Sodium chloride salt was purchased from VWR and used as received. PPO was sulfonated as previously reported to yield highly sulfonated sPPO.[24]

*Electrospun Mats*: The electrospinning apparatus, similar to that previously reported, consisted of two aluminum disks 10 cm in diameter oriented parallel to each other and separated by distance of 35 cm.[27] A 30 vol% solution of PA 6(3)T was delivered with a syringe pump (Harvard Apparatus PHD 2000) at a rate of 0.01 mL $min^{-1}$ to a 1.0 mm ID needle in the top aluminum disk. A high voltage power supply (Gamma High Voltage Research, ES40P) provided a 34 kV potential to the upper aluminum disk in contact with the solution. Under these conditions, an electrospun mat about 100-μm thick could be produced in 2 h. PCL electrospun mats were made using the same setup from a 10% solution of polymer in chloroform and methanol (3:1 by weight). The PCL mats had an average fiber diameter of 8.6 ± 0.8 μm, while the PA 6(3)T mats had an average fiber diameter of 1.24 ± 0.17 μm. Similar fibers and mats have been produced and characterized previously.[35–37]

*LbL Dip Assembly (Dip-LbL)*: Electrospun mats about 1" × 2" in size were placed into home-built plastic sample holders to ensure the sample remained planar during assembly. LbL assembly utilized a programmable ZEISS DS50 slide stainer. The mats were immersed in PDAC solution for 15 min, followed by three two minute rinses in water, and then placed in sPPO solution for 15 min, followed by three two minute rinses in water; the process was repeated numerous times to yield thick coatings. The PDAC and sPPO solutions were both 10 mM based on the molecular weight of repeat units. All polymer and rinse solutions for dip-LbL had pH 1. The composite membranes were rinsed in deionized water after assembly to remove excess ions from the films. Various concentrations of sodium chloride were added to polyelectrolyte and rinse solutions to control the growth characteristics and transport properties of the LbL film.

*LbL Spray Assembly (Spray-LbL)*: Electrospun mats about 4" × 4" in size were placed onto a 3" diameter plastic funnel fitted with a steel mesh for support. Sprayed films were fabricated using the same polymer and rinse solutions described above. The mats were plasma-etched in oxygen for 45 s and soaked in the PDAC solution for 5 min before spraying. A home-built automated spraying setup, as previously detailed, was used to coat the mats.[31] An automated program run by a logic relay controlled the apparatus, spraying the PDAC and sPPO solutions for 3 s each, with 5 s of rinse water spray in between the polymer sprays. The process was repeated for the desired number of bilayers. For some samples, a vacuum was applied to the back of the electrospun mat using a venturi pump supplied with nitrogen at 50 psi (vacuum-assisted spray-LbL). Free-standing LbL films were assembled on Teflon substrates or polystyrene-coated silicon wafers and gently peeled off after assembly, similar to a previous report.[38]

*Characterization*: SEM images were obtained on a JEOL JSM-6060 scanning electron microscope after coating the composite membranes with 5 nm of Au/Pd. Cross-sectional images were obtained by cryofracturing composite membranes in liquid nitrogen. Protonic conductivity measurements of the coated electrospun mats were made by cutting 1 cm × 2 cm samples, soaking them in pH 2 water and then rinsing with deionized water so that only protons associated with the sulfonic acid groups are available to contribute to the measured conductivity, and placing them in a conductivity cell with two platinum wires 1 cm apart as the electrodes. Temperature and humidity were controlled using a chamber from Electro-tech Systems, Inc. Impedance values were determined by electrochemical impedance spectroscopy with a Solartron 1260 impedance analyzer, measuring from 100 kHz down to 10 Hz. The thickness of the composite membrane was measured using cross-sectional imaging on an optical microscope and confirmed by a micrometer with 0.5 N applied force. Methanol permeability values were determined by using a dual chamber apparatus, where the membrane sample is the separator between pure methanol and water. The chambers were stirred, and the increase in methanol concentration of the water as a function of time was determined by the changes in the refractive index of the solution using a Waters 2414 Refractive Index Detector. Uniaxial tensile tests were conducted on 100 mm × 25 mm rectangular specimens of coated electrospun mats, at ambient conditions and constant engineering strain rate, with an EnduraTEC Electroforce 3200 in displacement control mode. "Wet" state experiments were conducted by saturating the specimens with deionized water once they were in the tensile fixture and testing immediately. Axial and transverse strains were measured with a Qimaging Retiga 1300 video camera in conjunction with Vic2D video extensometer software. The force-displacement data as taken from the Electroforce and the video extensometer, respectively, were reduced to true stress-true strain results assuming isotropic incompressible behavior. True stress is defined as the ratio of force to current (deformed) cross-sectional area and true strain is defined as the natural logarithm of the ratio of current length to original length (length being the axial distance between video-imaged marks).

## Acknowledgements

This work was supported by the National Science Foundation - Engineering Division Award #0700414, Masdar Institute of Science and Technology, and the Samsung Advanced Institute of Technology. We thank Joe Lowery for help preparing PCL electrospun mats, and Chia-Ling Pai for helpful discussions around electrospinning. We also thank Jung-Ah Lee for help obtaining cross-sectional SEM images, and Sarah Rumbley and Marie Burkland for their assistance in assembling the spray composite membranes and taking methanol permeability measurements. We thank the MIT Institute of Soldier Nanotechnology for use of facilities.

Received: October 5, 2012
Published online: January 18, 2013

[1] F. de Bruijn, *Green Chem.* **2005**, *7*, 132.
[2] S. G. Chalk, J. F. Miller, *J. Power Sources* **2006**, *159*, 73.
[3] M. Doyle, G. Rajendran, in *Handbook of Fuel Cells: Fundamentals, Technology and Applications*, Vol. *1* (Eds: W. Vielstich, A. Lamm, H. A. Gasteiger), John Wiley & Sons, Chichester, England **2003**, p. 351.
[4] J. Wu, X. Z. Yuan, J. J. Martin, H. Wang, J. Zhang, J. Shen, S. Wu, W. Merida, *J. Power Sources* **2008**, *184*, 104.
[5] M. Inaba, T. Kinumoto, M. Kiriake, R. Umebayashi, A. Tasaka, Z. Ogumi, *Electrochim. Acta* **2006**, *51*, 5746.
[6] R. Borup, J. Meyers, B. Pivovar, Y. S. Kim, R. Mukundan, N. Garland, D. Myers, M. Wilson, F. Garzon, D. Wood, P. Zelenay, K. More, K. Stroh, T. Zawodzinski, J. Boncella, J. E. McGrath, M. Inaba, K. Miyatake, M. Hori, K. Ota, Z. Ogumi, S. Miyata, A. Nishikata, Z. Siroma, Y. Uchimoto, K. Yasuda, K. I. Kimijima, N. Iwashita, *Chem. Rev.* **2007**, *107*, 3904.

[7] Y.-H. Lai, C. K. Mittelsteadt, C. S. Gittleman, D. A. Dillard, *J. Fuel Cell Sci. Technol.* **2009**, *6*, 021002.
[8] F. Bauer, S. Denneler, M. Willert-Porada, *J. Polym. Sci., Part B: Polym. Phys.* **2005**, *43*, 786.
[9] R. Solasi, Y. Zou, X. Huang, K. Reifsnider, D. Condit, *J. Power Sources* **2007**, *167*, 366.
[10] A. Kusoglu, A. M. Karlsson, M. H. Santare, S. Cleghorn, W. B. Johnson, *J. Power Sources* **2006**, *161*, 987.
[11] X. Huang, R. Solasi, Y. Zou, M. Feshler, K. Reifsnider, D. Condit, S. Burlatsky, T. Madden, *J. Polym. Sci., Part B: Polym. Phys.* **2006**, *44*, 2346.
[12] R. C. McDonald, C. K. Mittelsteadt, E. L. Thompson, *Fuel Cells* **2004**, *4*, 208.
[13] F. Liu, B. Yi, D. Xing, J. Yu, H. Zhang, *J. Membr. Sci.* **2003**, *212*, 213.
[14] K. M. Nouel, P. S. Fedkiw, *Electrochim. Acta* **1998**, *43*, 2381.
[15] T. L. Yu, H. L. Lin, K. S. Shen, L. N. Huang, Y. C. Chang, G. B. Jung, J. C. Huang, *J. Polym. Res.* **2004**, *11*, 217.
[16] J. J. Shi, B. Jang, *J. Fuel Cell Sci. Technol.* **2011**, *8*, 014501.
[17] Y.-H. Liu, B. Yi, Z.-G. Shao, D. Xing, H. Zhang, *Electrochem. Solid-State Lett.* **2006**, *9*, A356.
[18] E. Chalkova, M. V. Fedkin, D. J. Wesolowski, S. N. Lvov, *J. Electrochem. Soc.* **2005**, *152*, A1742.
[19] C. Yang, P. Costamagna, S. Srinivasan, J. Benziger, A. B. Bocarsly, *J. Power Sources* **2001**, *103*, 1.
[20] G. Decher, *Science* **1997**, *277*, 1232.
[21] G. Decher, J. D. Hong, J. Schmitt, *Thin Solid Films* **1992**, *210*, 831.
[22] P. T. Hammond, *Adv. Mater.* **2004**, *16*, 1271.
[23] T. R. Farhat, P. T. Hammond, *Adv. Funct. Mater.* **2005**, *15*, 945.
[24] A. A. Argun, J. N. Ashcraft, P. T. Hammond, *Adv. Mater.* **2008**, *20*, 1539.
[25] J. N. Ashcraft, A. A. Argun, P. T. Hammond, *J. Mater. Chem.* **2010**, *20*, 6250.
[26] J. Doshi, D. H. Reneker, *J. Electrost.* **1995**, *35*, 151.
[27] Y. M. Shin, M. M. Hohman, M. P. Brenner, G. C. Rutledge, *Polymer* **2001**, *42*, 09955.
[28] G. C. Rutledge, S. V. Fridrikh, *Adv. Drug Delivery Rev.* **2007**, *59*, 1384.
[29] S. V. Fridrikh, J. H. Yu, M. P. Brenner, G. C. Rutledge, *Phys. Rev. Lett.* **2003**, *90*, 144502.
[30] J. Choi, K. M. Lee, R. Wycisk, P. N. Pintauro, P. T. Mather, *J. Mater. Chem.* **2010**, *20*, 6282.
[31] K. C. Krogman, N. S. Zacharia, S. Schroeder, P. T. Hammond, *Langmuir* **2007**, *23*, 3137.
[32] K. C. Krogman, J. L. Lowery, N. S. Zacharia, G. C. Rutledge, P. T. Hammond, *Nat. Mater.* **2009**, *8*, 512.
[33] S. Kundu, L. C. Simon, M. Fowler, S. Grot, *Polymer* **2005**, *46*, 11707.
[34] W. M. Deen, *Analysis of Transport Phenomena*, Oxford Univeristy Press, **1998**.
[35] J. L. Lowery, N. Datta, G. C. Rutledge, *Biomaterials* **2010**, *31*, 491.
[36] C.-L. Pai, M. C. Boyce, G. C. Rutledge, *Polymer* **2011**, *52*, 2295.
[37] M. M. Mannarino, G. C. Rutledge, *Polymer* **2012**, *53*, 3017.
[38] J. L. Lutkenhaus, K. D. Hrabak, K. McEnnis, P. T. Hammond, *J. Am. Chem. Soc.* **2005**, *127*, 17228.